


Please cite the Published Version

Netto, TR, Evans, AK, Goddard, DT, Cooper, JL and Kelly, P  (2025) Effects of sample bias on wear resistance of magnetron sputtered chromium coated zirconium alloy. Surface and Coatings Technology, 498. 131847 ISSN 0257-8972

DOI: <https://doi.org/10.1016/j.surfcoat.2025.131847>

Publisher: Elsevier BV

Version: Published Version

Downloaded from: <https://e-space.mmu.ac.uk/638442/>

Usage rights:  [Creative Commons: Attribution 4.0](https://creativecommons.org/licenses/by/4.0/)

Additional Information: This is an open access article which first appeared in Surface and Coatings Technology, published by Elsevier

Data Access Statement: Data will be made available on request.

Enquiries:

If you have questions about this document, contact openresearch@mmu.ac.uk. Please include the URL of the record in e-space. If you believe that your, or a third party's rights have been compromised through this document please see our Take Down policy (available from <https://www.mmu.ac.uk/library/using-the-library/policies-and-guidelines>)



Effects of sample bias on wear resistance of magnetron sputtered chromium coated zirconium alloy[☆]

Thais R. Netto^{a,*}, Adele K. Evans^a, David T. Goddard^b, Jack L. Cooper^b, Peter Kelly^a

^a Surface Engineering Group, Manchester Metropolitan University, Chester Street, Manchester M1 5GD, UK

^b National Nuclear Laboratory, Preston Laboratory, Springfields, Preston, Lancashire PR4 0XJ, UK

ARTICLE INFO

Keywords:

Accident-tolerant fuel (ATF)
Chromium coating
Wear resistance
Magnetron sputtering

ABSTRACT

Research on accident-tolerant fuels (ATFs) for Light Water Reactors (LWRs) has focused on improving the safety of zirconium alloy fuel rods since the Fukushima accident in 2011. Additionally, normal LWR operating conditions cause fretting wear on the fuel rod surface, which requires tribological improvements. Chromium-based coatings on zirconium alloys are one of the most advanced concepts for developing a fuel that can withstand accidents. Both under operating conditions and when subjected to high-temperature steam, Zr alloys with protective coatings demonstrated improvements, compared to uncoated surfaces. This study aims to evaluate the effect of substrate bias on the structure and tribological properties of chromium films deposited by magnetron sputtering onto Zr alloy nuclear fuel rod cladding. The coatings were also characterised by scanning electron microscopy (SEM), energy dispersive X-ray spectroscopy (EDX), X-ray diffraction (XRD), atomic force microscopy (AFM), transmission electron microscopy (TEM) and optical profilometry. The hardness of the coating was measured with a nano-indenter. Initial finding indicates that the application of a low substrate bias of -50 V enhances film density and adhesion and also reduces the coating wear rates, in comparison to higher biases (-100 V to -150 V) or no applied bias.

1. Introduction

Concerns about global warming in the last few years have led to more than 100 countries committing to achieving carbon neutrality by 2050 or 2060 [1]. A key element of achieving this is the improvement and development of clean and renewable energy systems to replace fossil fuels. Nuclear energy is a potential candidate for clean energy because it is considered a low-carbon energy source. Very low emissions of CO₂ are produced in the nuclear fuel life cycle, e.g., through mining, transportation, and fuel fabrication. However, no greenhouse gases are produced during the nuclear plant operation [2,3].

Like any other energy source, nuclear power also has its challenges. Safety is one of the main concerns and it is preeminent to successful operation. The fuel systems are usually uranium pellets loaded inside 4 m long tubes, or cladding, made of zirconium-based alloys [4]. The fuel rod cladding is a key safety component as it is the first barrier to protect the fuel and fission products from the environment, and one of the main problems faced in the daily operation of nuclear plants is the failure of

the cladding. A survey carried out by Kim [5] showed that about 65 % of fuel rod failures are caused by the phenomenon called grid-to-rod fretting (GTRF).

This phenomenon occurs in the reactor's nuclear core, more precisely, where the fuel claddings are held in a spacer grid assembly. The coolant flows through the assembly and induces a vibration at the grid-to-rod interface. This repeated movement over long time periods causes a gradual relaxation of the grid, increasing the gap between the cladding and the grid [6]. As a result, there is a significant increase of fretting motion between the surfaces, which leads to fatigue problems, stress corrosion cracking and wear damage [7–10]. Debris trapped at the grid-to-rod interface can also cause three body abrasion issues.

Many studies have focused on reducing accidents and contributing to improvements in the safety of nuclear energy. In this context, the Accident-Tolerant Fuels (ATF) concept was created to reduce the chance of fuel failure during normal operation; to improve the fuel's performance under accident conditions; and to minimise the consequences of accidents [11]. Investigations around other materials or the

[☆] This article is part of a special issue entitled: Multifunctional Coatings published in Surface & Coatings Technology.

* Corresponding author.

E-mail address: T.Netto@mmu.ac.uk (T.R. Netto).

¹ Present address: Manchester Metropolitan University, Chester Street, Manchester, M1 5GD, UK.

development of advanced materials could be a future solution to the existing issues with Zr alloy fuel rods. An effective near-term solution, though, is coating the exterior of the Zr alloy cladding with a thin layer of an alternate material to provide enhanced protection [12]. This option is faster to implement than developing and employing a new cladding material, and it also takes advantage of the existing zirconium-based rods properties [13]. Furthermore, some previous studies demonstrate significant results for the coated Zr alloys, such as a higher melting point, corrosion and wear resistance improvements, and lower hydrogen generation at elevated temperatures [4,14]. Recent research suggests that chromium-based coatings on zirconium alloys are one of the most advanced concepts for developing a fuel that can withstand accidents [11,15–18]. The chromium coating's properties lead to several improvements in the cladding performance in terms of oxidation and wear protection [19]. For example, Reed [20] used an autoclave rig to simulate the nuclear reactor and evaluate the wear resistance of the Cr-based coatings. They argue that Cr-coatings improved by at least 80 % the cladding's wear resistance in comparison to the ZIRLO™ substrate. Also, a more than 50 % wear reduction in the as-received ZIRLO™ grid has been reported. The conclusions of this study are that the improvements may be related to chromium's higher hardness and the minimisation of adhesive wear by not rubbing against similar materials. Zhao [21] investigated the corrosion behaviour of Zr alloy in a simulated reactor environment using an autoclave. The study compared uncoated Zr alloy with Zr alloy coated with Cr. The results showed that the wear depth, wear volume, and wear coefficient were reduced by approximately 3 to 5 times when the Cr coating was applied.

Coating properties are highly associated with their deposition method and parameters, which can be adjusted according to the film's application. Among the deposition techniques available, magnetron sputtering is an attractive technology for this application because it produces high quality films with dense structures [22,23] and is readily scalable. During the magnetron sputtering deposition process, increasing the bias voltage applied to the substrate is an option known to produce denser structures [24,25]. Biasing the substrate results in the acceleration of positive ions (predominantly argon ions) in the plasma towards the samples. The higher energy of the Ar ions incident at the substrate induces a compressive stress, creating a denser coating that may be beneficial regarding mechanical resistance. However, excessive biasing can result in higher film stresses, with possible cracking and delamination of the film [26,27].

A denser structure is a desired property for a coating deposited onto nuclear fuel rods to improve their wear protection and furthermore, to act as a barrier layer to oxidation. For this reason, a deeper understanding of the influence substrate bias on the properties and mechanical resistance of the Cr coatings is necessary to implement them safely in the nuclear plant environment. Therefore, this study aims to evaluate the effect of bias on the structure and wear resistance of chromium films deposited via magnetron sputtering.

2. Experimental

2.1. Coating deposition process

The coating deposition runs were conducted in a sputtering rig in which a single unbalanced magnetron was installed in the chamber roof in the sputter down configuration. A chromium target (99.99 % purity), 300 × 100 mm in size was fitted to the magnetron. The substrates were ZIRLO™ alloy coupons, sized 30 × 20 × 1 mm³, which were ultrasonically pre-cleaned in acetone for 10 min prior to deposition. The substrates were placed 10 cm below the magnetron on a sample holder that was rotated during deposition to ensure uniform thickness of the Cr coatings. The magnetron was powered by an Advanced Energy Pinnacle Plus power supply in pulsed DC mode, operating at 100 kHz and 80 % duty. All the samples were sputter cleaned for 15 min at –650 V before the deposition, and the working pressure was 0.36 Pa. Samples were

coated with no bias applied (NBA), i.e., at floating potential, followed by applied DC biases of –50 V, –100 V, and –150 V. After the deposition runs, the substrates were allowed to cool down before the chamber was vented and the substrates removed. Run times were selected based on previous experience to give coating thicknesses in the range 6–7 μm to suit their intended application.

2.2. Characterisation techniques

The film topography was assessed using a FIB-SEM (Zeiss Crossbeam 350) and an AFM (Horiba Xplora plus V1.2), which also provided a measure of surface roughness. In preparation for TEM analysis, samples were milled in cross section using a focused ion beam (FIB). Prior to milling, a platinum layer was deposited on the area of interest on the coating surface to maintain the integrity of the coating during ion milling. Then, for an in-depth characterisation of the coating layer, scanning TEM (STEM) was used (TESCAN Tensor) operated at 100 kV. The crystallinity and grain sizes of the films were examined by an X-ray diffractometer (Malvern Panalytical Xpert), with Cu K_α radiation at 0.154 nm, over a scan range from 5 to 100° 2θ. The accelerating voltage and applied current were set to 40 kV and 30 mA, respectively.

The coating hardness (H) was measured using a nano-indenter (Anton Paar – Nanoindentation tester: NHT³). The applied maximum load was 50 mN, and the loading rate was 33 nm.s^{–1} for all measurements, which ensured that the maximum penetration depth was less than 10 % of the film thickness. After indentation, the results were analysed using Oliver and Pharr's theory to obtain the hardness values.

2.3. Tribology test

Since a fretting wear option was not available, the wear tests were conducted in a tribometer using linear reciprocating movement (TRB3 Tribometer, Anton Paar) to mimic the grid-to-rod phenomenon, although with a much greater amplitude. The experiments were carried out in an ambient environment using a 6 mm diameter AISI 316 stainless steel ball. Coatings were tested at three loads: 3, 4 and 5 N, at a frequency of 10 Hz with a full amplitude of 4 mm. The total test distance was 50 m, accounting for 10 min tests. The tests were repeated three times at each load used. The wear depths and wear volume were measured using a white light interferometer Profilm3D (Filmetrics). Also, the wear tracks were analysed in the EDX (Hitachi TM4000).

The specific wear rate (W_s) was calculated as defined [28]: the wear volume of the material (V), divided by the applied normal load (N), and sliding distance (D), as detailed in Eq. (1):

$$W_s = \Delta V / ND \quad (1)$$

The wear volume was estimated as previously described in Reed [20] using Eq. (2):

$$V = AD \quad (2)$$

where A indicates the cross-section worn area (μm²) and D is the sliding distance (4 mm).

3. Results

3.1. Microstructure characterisation

Fig. 1 presents the top surface SEM images of selected coatings. As can be seen in the images, the surface morphology differs significantly in shape and grain size, depending on the bias voltage used. The no bias applied (NBA) coating (1a) exhibited pyramid shaped grains of varying sizes that originated from the columnar structure. In addition, gaps or pores can be observed between the columns. Increasing to –50 V bias voltage (1b) significantly changes the coating structure, with the surface morphology becoming smoother and denser (Ra values of surface

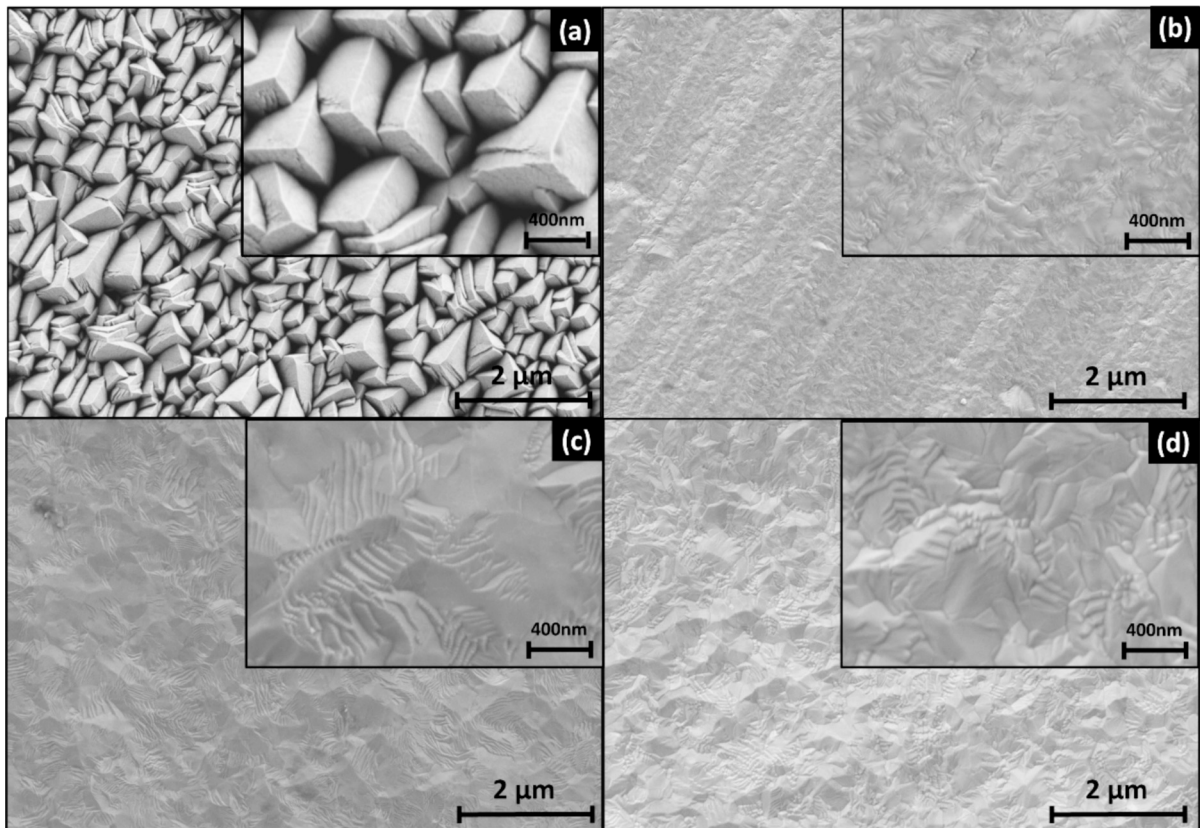


Fig. 1. SEM top surface images of chromium coatings deposited with (a) NBA, (b) -50 V, (c) -100 V and (d) -150 V bias.

roughness, measured by AFM are listed in Table 1). It can also be noticed that forming lines on the surface of the substrate are reproduced on the coating surface, meaning the coating is highly conformal to the substrate. When the voltage is increased to -100 V, (1c) the surface is even smoother, and still dense and remains this way at -150 V bias (1d). Although the surface is continuous and uniform, defined boundaries and grains are formed on the surface. These results might be a consequence of the high-energy of the incident ion bombardment that leads to a higher mobility of the atoms at the surface with small grains merging, resulting in a larger grain size [29,30].

The FIB milled section images of each deposition are presented in Fig. 2. In agreement with the top surface images (see Fig. 1), the NBA sample (2a) presented a porous columnar structure. Meanwhile, the films coated with -50 V (2b), -100 V (2c) and -150 V (2d) bias voltages demonstrated much denser structures, though some element of a dense columnar structure is still visible.

As detailed in Table 1, the NBA coating had a net deposition rate of $1.23 \mu\text{m/h}$, which decreased progressively with applied bias from 1.13 to $0.85 \mu\text{m/h}$ at bias voltages of -50 , -100 and -150 V, respectively. Thus, the deposition time was increased for the -150 V sample from 6 h to 8 h to compensate for the reduced net deposition rate measured for this sample.

Fig. 3 presents the STEM images of the Cr coatings deposited under

Table 1

Coating time, thickness, deposition rate and roughness of the NBA, -50 V, -100 V and -150 V Cr coatings.

Sample ID	Coating time (h)	Thickness (μm)	Net deposition rate ($\mu\text{m/h}$)	AFM roughness Ra (nm)
NBA	6 h	6.9 ± 0.2	1.23	31.1 ± 5.7
-50 V	6 h	6.8 ± 0.1	1.13	19.6 ± 7.1
-100 V	6 h	6.3 ± 0.4	1.05	15.3 ± 3.2
-150 V	8 h	6.8 ± 0.1	0.85	17.3 ± 2.1

bias voltages of (a) NBA, (b) -50 V, (c) -100 V, and (d) -150 V.

Voids or gaps can be seen between the columnar grains in the STEM image of the NBA coating Fig. 3(a), whereas the biased coatings all show continuous structures (Fig. 3(b) to (d)). Measurements of the lengths and widths of the grains were made from the latter three samples using the image analysis software, ImageJ. The average grain sizes ($n = 20$) and grain aspect ratios for these samples are presented in Table 2. The grain aspect ratio gives an indication of the shape of the grains: an aspect ratio closer to 1 indicates a more circular shape, while lower values suggest a more columnar grain structure.

A significant change in grain size and shape was observed in response to the different bias voltages applied, as evidenced by the STEM analyses. First, the NBA sample exhibited a voided columnar structure, with no grain boundaries between these columns. For the coatings deposited with applied bias voltages, voids are removed and the structures are densified. The grains are elongated in shape, particularly in the -150 V Cr coating, which showed the lowest aspect ratio (the ratio between the width and length of the grain). Regarding the effect of bias voltage on grain size, the analyses revealed much smaller grains in the -50 V coating. As the bias voltage increased, the grains became larger and more elongated. The grain size (i.e. width) of the Cr coating deposited at -50 V was less than half that of the coating deposited at -100 V, measuring 80 nm and 171 nm, respectively. Meanwhile, the grain size of the coating deposited at -150 V was a further 20 nm larger than those in the -100 V sample.

Similar findings were reported in the study by Zhu [31], which examined the effects of bias voltage on the microstructure and steam oxidation behaviour of sputtered Cr coatings. They tested Cr coatings under no bias and at bias voltages of -50 V, -100 V, and -150 V, observing a gradual increase in grain size with increasing bias voltage. They attributed the influence of bias voltage on grain size to two primary factors. First, a negative bias introduces more defects into the matrix due to ion bombardment, leading to an increased number of nucleation sites

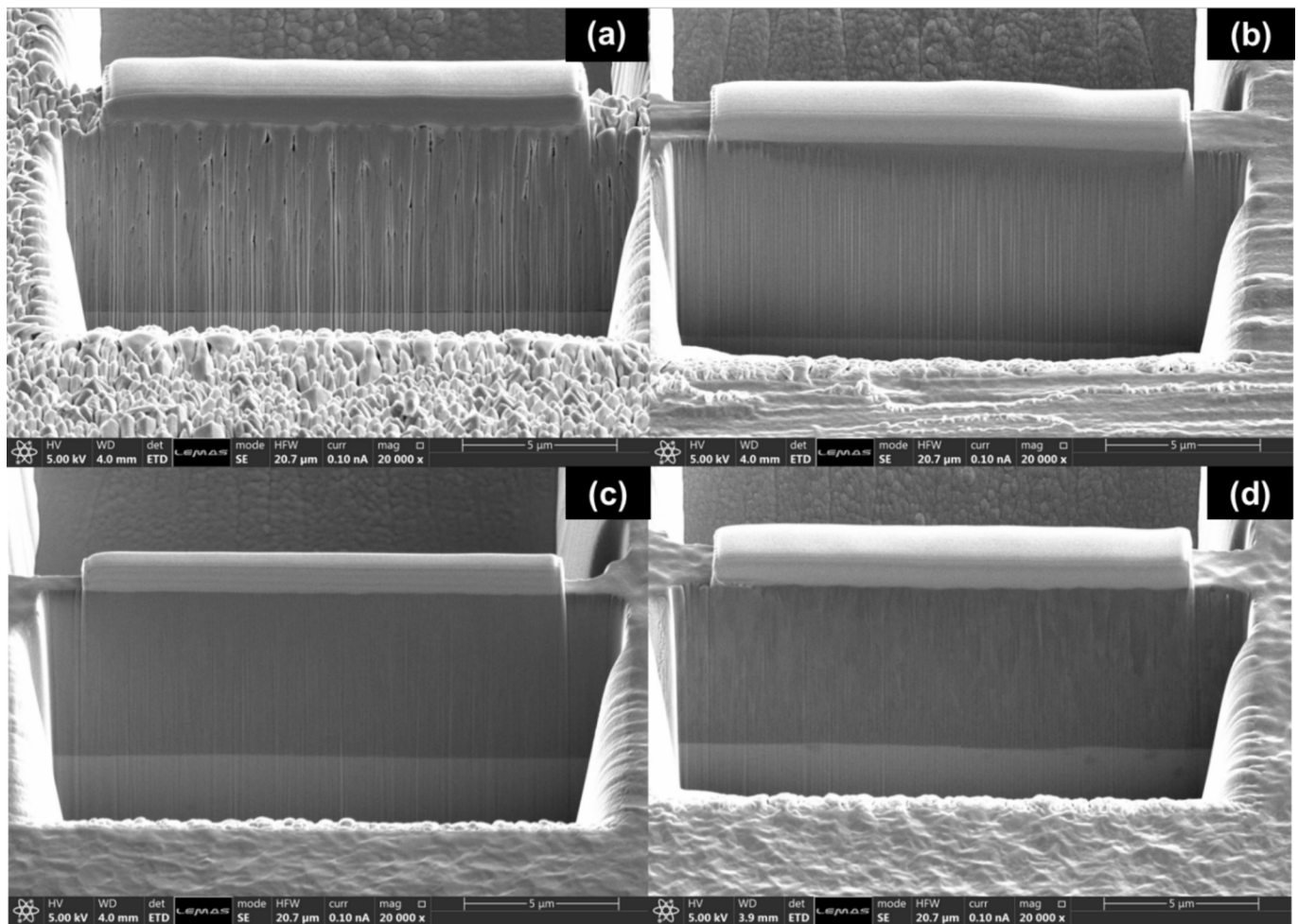


Fig. 2. Cross-section images of chromium coatings deposited with (a) NBA, (b) -50 V, (c) -100 V, and (d) -150 V.

and smaller grains. Second, higher bias voltage can raise the substrate temperature, enhancing the diffusion capability of atoms and grain boundaries, which promotes grain fusion and increases grain size. Consequently, the dominant factor contributing to grain size growth is the elevated substrate temperature [31].

The X-ray diffraction patterns for these coatings are shown in Fig. 4. All the films presented a peak at around $2\theta = 44.3^\circ$, corresponding to the Cr (110) peak, although for the NBA sample, the (110) peak is very low intensity and barely imperceptible when shown on the same scale as the applied biased samples, hence the insert showing the peak region magnified for this sample. In addition, coatings deposited at -50 V, -100 V, and -150 V bias presented lower intensity peaks corresponding to the (200) and (211) planes at about $2\theta = 64.5^\circ$ and 81.7° (PDF card, 85–1336). Comparing the relative peak heights for the (110), (200) and (211) and the reference values for chromium, indicates that the -50 V coating showed the strongest (110) texture.

The nano-hardness results revealed relevant findings about the influence of the different bias voltages, as detailed in Table 3. The NBA coating showed the lowest hardness at 3.5 GPa, in comparison with the other Cr films, indeed this value was lower than that recorded for the Zr alloy substrate. In contrast, the -50 V bias coating presented the highest hardness among the samples at 12 GPa. At the higher bias voltages of -100 V and -150 V, the hardness was observed to decrease to 7–8 GPa.

The elasticity modulus data exhibited a slightly different trend (see Table 3), although the NBA coating again had the lowest value of 149 GPa. In this case, the remaining coatings all had broadly similar values in the range 284 to 318 GPa, with no clear trend with increasing bias voltage.

Another parameter of interest is the H/E ratio, which has been reported as a tool to assess the wear resistance of materials, especially coatings, with a high H/E ratio considered to be an indicator of good wear resistance in a coating [32]. As can be seen in Table 3, the -50 V bias voltage coating presented the highest H/E ratio, with the other coatings fluctuating around a similar ratio.

3.2. Mechanical properties assessments

Fig. 5 displays a chart (a) displaying the wear rate calculated for each sample and load used, and a line chart (b) illustrating wear depth vs. the load. Each chart in Fig. 5 show the standard deviation bars to describe the variability in the data. In addition, Fig. 6 exhibits the 3D morphology images of the wear track for each film and load used.

As can be seen in both charts, a notable enhancement is observed when employing Cr films compared to the uncoated sample. The ZIRLO™ showed a high wear rate (about $6 \text{ mm}^3/\text{Nm}$) and a wear penetration depth of around $30 \mu\text{m}$ for all loads tested. As observed in the graphs and image, none of the coated samples showed wear rates or depths as high as these values.

Among the Cr-coated samples, the NBA condition showed the poorest protection and was rapidly worn through at the higher test loads. This condition presented the highest wear rate for the coated samples, and the wear depth was the greater in comparison with the other Cr films. However, it still offered some protection to the substrate when compared with the bare substrate. Therefore, even a porous and columnar Cr-coating performed better than no film. On the other hand, the best performance was the -50 V bias film, as no signs of wear were

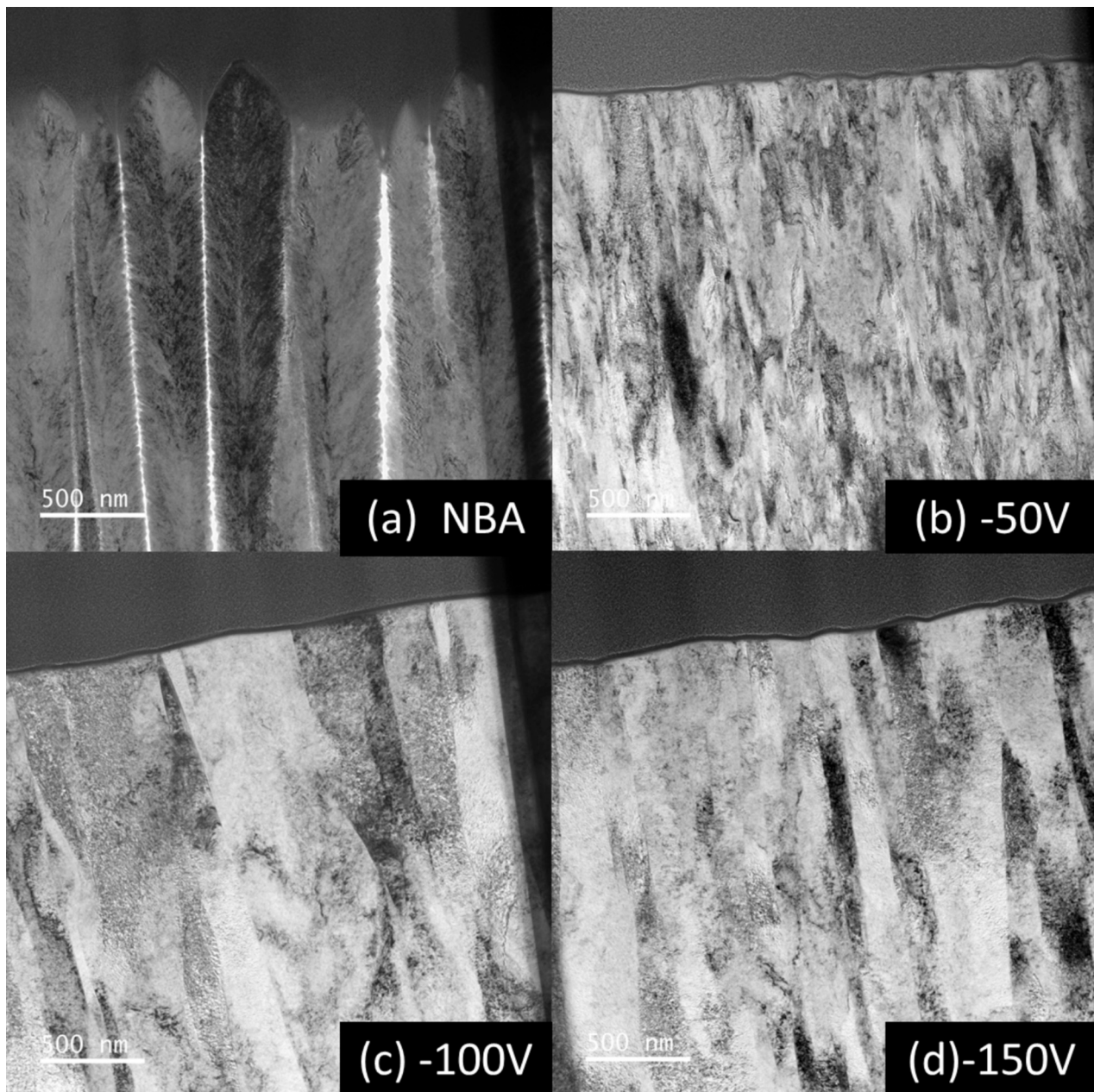


Fig. 3. STEM images of the cross-sections of Cr coatings deposited under bias voltages of (a) NBA, (b) -50 V, (c) -100 V, and (d) -150 V.

Table 2

Grain size and grain aspect ratio of the cross-sections of Cr coatings deposited under bias voltages of (a) -50 V, (b) -100 V, and (c) -150 V.

Sample ID	Grain size (nm)	Grain aspect ratio
-50 V	80 ± 42	0.4 ± 0.2
-100 V	171 ± 89	0.5 ± 0.3
-150 V	190 ± 59	0.2 ± 0.1

detected on the surface, leading to zero measurable wear rate over the range tested.

Next, the deposition at -100 V bias voltage presents modest wear at 3 and 4 N, but this film still protects the substrate. However, at 5 N the -100 V coating is seriously damaged. The wear track penetrated nearly $15 \mu\text{m}$ into the sample, which is much greater than the coating thickness ($6.3 \mu\text{m}$). Finally, when the bias increased to -150 V, although gradual wear climbed with increasing load, the film protected the substrate even

at 5 N. This coating also exhibits a very low, but measurable wear rate.

Fig. 7 presents the EDX mapping of wear tracks from the 5 N friction test on Cr-coated samples subjected to -50 V and -100 V bias voltages, which exhibited contrasting behaviours. In the EDX maps, the Cr coating is represented in blue, iron from the ball bearing is shown in pink, and Zr from the substrate is presented in green. For the sample coated at -50 V bias, no surface wear was observed, and consequently, no Zr was detected. In contrast, the sample coated at -100 V bias exhibited significant wear under the 5 N load, reaching the substrate, evidenced by the Zr that was identified in the EDX analysis.

Fig. 8 presents the EDX mapping of the counterface ball scar from the 5 N friction test on Cr-coated samples subjected to -50 V and -100 V bias voltages. These samples were chosen again due to their contrasting behaviours. The EDX maps illustrate the distribution of Cr (blue), Fe (pink, from the ball bearing), Zr (green, from the substrate), and oxygen (red). Consistent with the findings in Fig. 7, the -50 V bias sample shows some wear on the ball bearing surface but no Zr detected. In

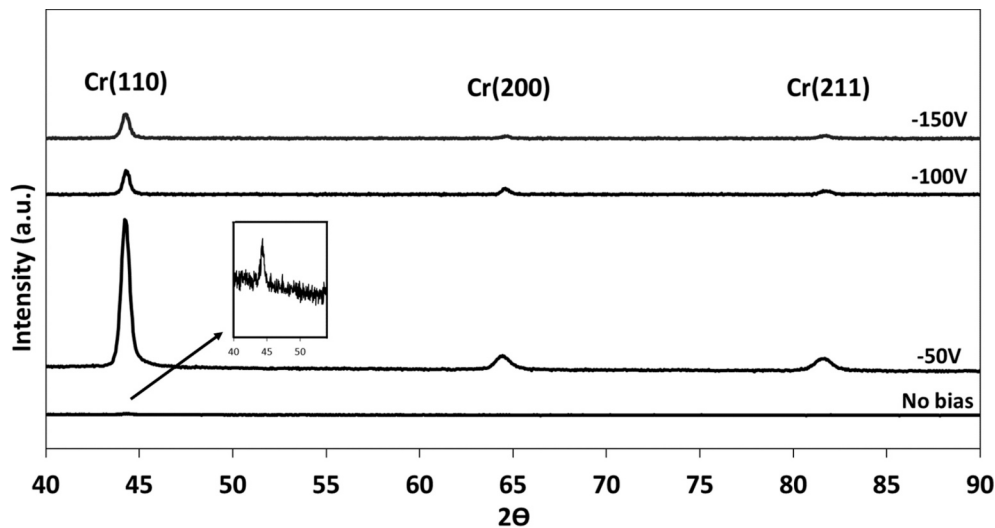


Fig. 4. X-ray spectra of Cr films coated at NBA, -50 V, -100 V and -150 V.

Table 3

Hardness, elastic modulus, and H/E ratio of the NBA, -50 V, -100 V and -150 V bias voltage Cr coating.

Sample ID	Hardness (GPa)	Elastic modulus (GPa)	H/E ratio
Zr uncoated	4.0 ± 0.8	118 ± 14	–
NBA	3.5 ± 0.6	149 ± 25	0.023
-50 V	12.1 ± 1.8	314 ± 46	0.039
-100 V	6.9 ± 1.0	318 ± 41	0.022
-150 V	7.8 ± 1.2	284 ± 33	0.027

contrast, a greater degree of wear is observed on the ball bearing of the -100 V bias sample, with Zr from the exposed substrate clearly detected.

Fig. 9(a) and (b) are SEM micrographs of the wear track regions for the 5 N load tests of the -50 V sample, whereas Fig. 9(c) and (d) show the same regions for the -100 V sample. Firstly, it can be seen in Fig. 9(a) and (c) that both worn surfaces present a darker trail along the wear direction. This darker contrast is the Fe accumulation on the surface, which was detected on the EDX analyses shown in pink (Fig. 7). The wear depth on the sample coated at -100 V bias voltage reached the substrate, as shown previously. As a consequence, in Fig. 9(d) noticeable, deep striations, or grooves are visible (lighter grey region) in the centre of the wear track of this sample, which represents the zirconium from the substrate identified on the EDX analyses. The -50 V sample only displays what looks like mild polishing in this region.

Regarding the wear features, both worn surfaces presented some debris accumulation among the wear tracks (shown by red arrows in Fig. 9), indicating adhesive wear. The debris are even more evident on the sample -100 V, in which the wear was more severe. Furthermore, in the sample -100 V also presents some fine and long parallel grooves at the coating's sliding surfaces along the friction direction (shown by red arrows in Fig. 9), which indicated signs of abrasive wear.

EDX mapping analyses were performed in the wear track regions of the 5 N test samples to identify the debris. The Cr-coatings at -50 V and -100 V bias voltage are shown in Fig. 10. As can be seen, zirconium is presented in green, iron in pink, chromium in blue and oxygen in red. The debris observed in darker spots inside the wear tracks appears to be iron from the counterface ball, as can be seen in pink in the EDX analyses (Fig. 10). Also, based on the Fe position, it seems that the iron debris are accumulating more over the chromium layers.

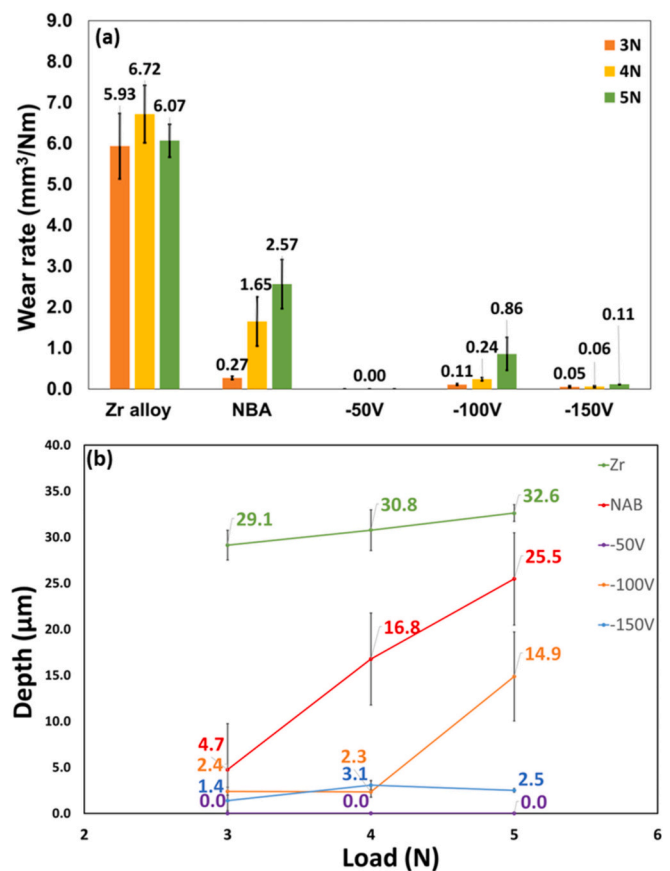


Fig. 5. (a) Wear rate, (b) wear depth of the uncoated ZIRLO™ and Cr-coated samples under NBA, -50 V, -100 V and -150 V bias voltage.

4. Discussion

4.1. Microstructure characterisation: influence of substrate bias

The application of a substrate bias voltage during the deposition of the chromium coatings produced in this work has had a profound influence on all of the properties investigated. Furthermore, an optimum bias voltage of -50 V was identified in many cases. The most obvious

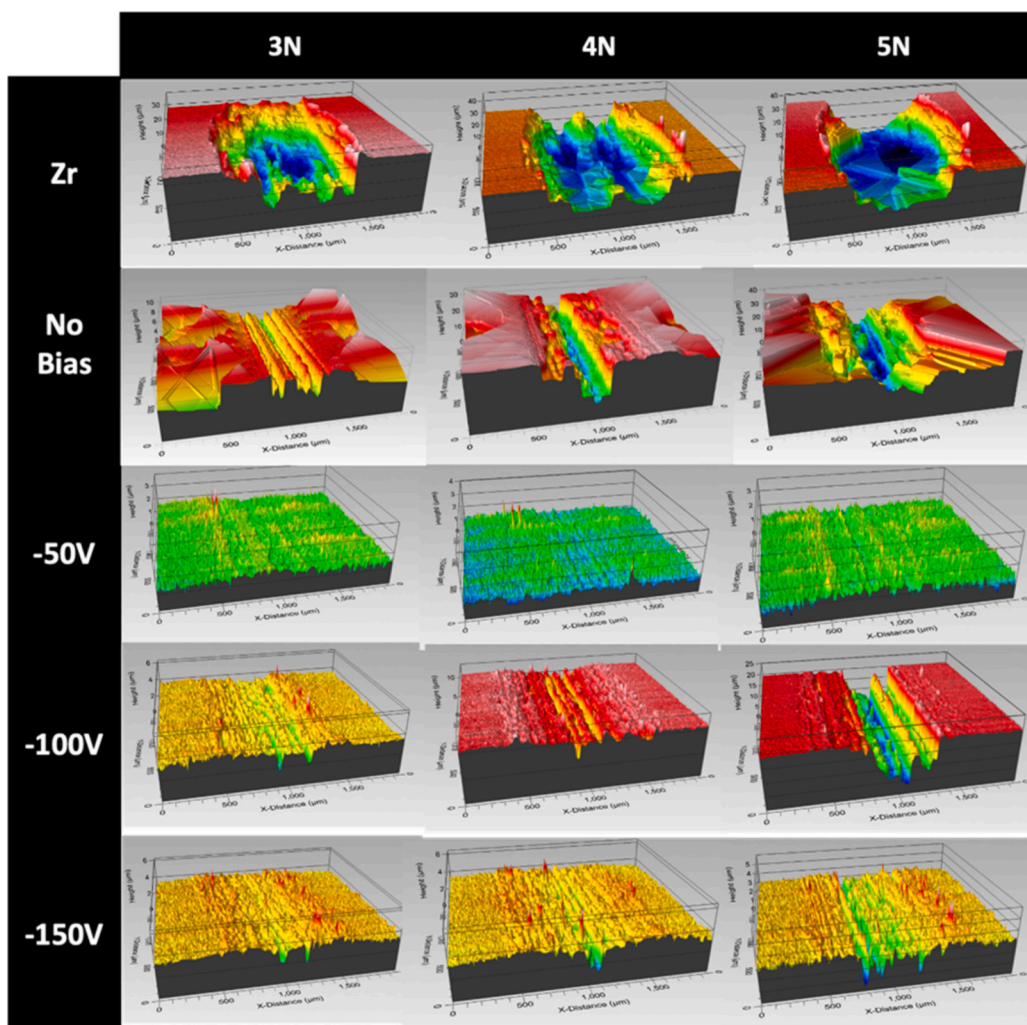


Fig. 6. Surface 3D morphology of the uncoated ZIRLO™ and Cr-coated samples under NBA, -50 V, -100 V and -150 V bias voltage.

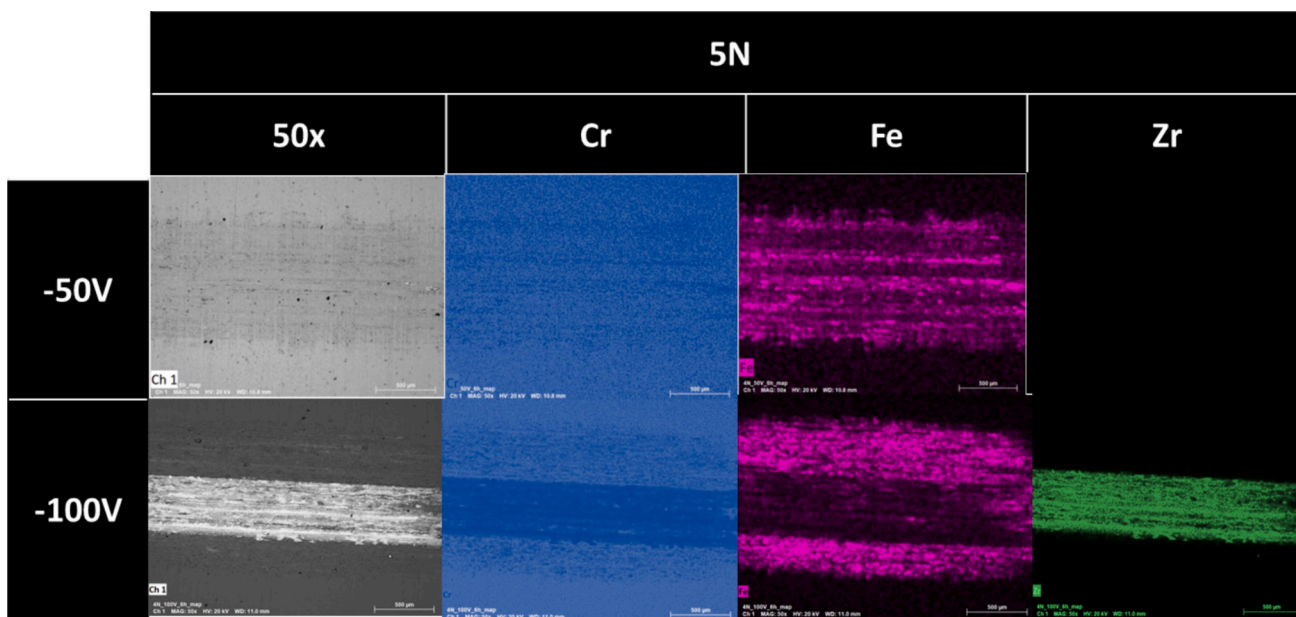


Fig. 7. EDX mapping of the wear track from the 5 N friction test on Cr-coated samples under -50 V and -100 V bias voltages.

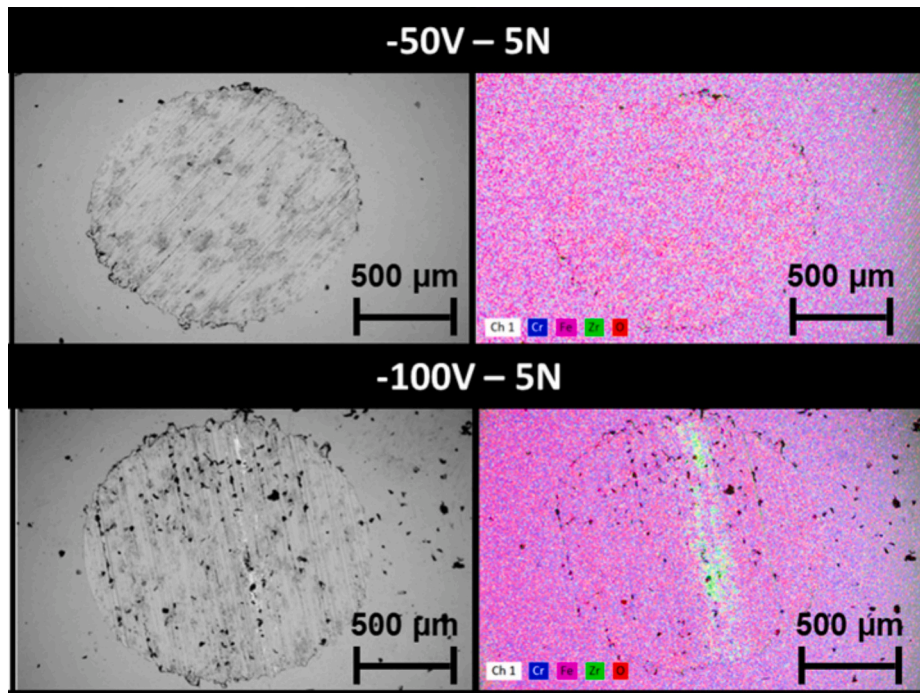


Fig. 8. EDX mapping on the ball scar of the uncoated ZIRLO™ and Cr-coated samples under NBA, -50 V, -100 V and -150 V bias voltage.

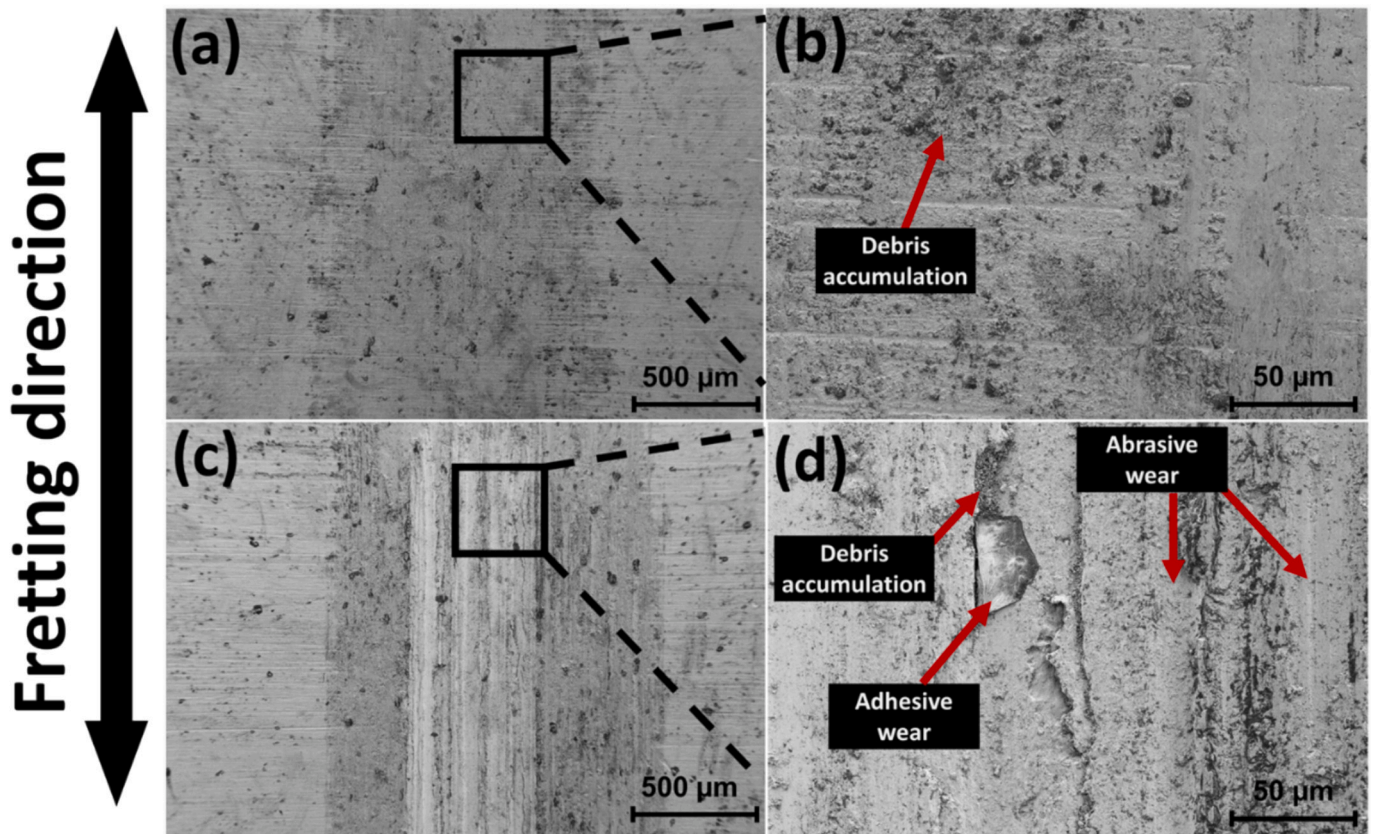


Fig. 9. SEM images of the wear track of the 5 N load test for Cr-coated samples under (a) and (b) -50 V; (c) and (d) -100 V bias voltage.

change is in the structure of the coating, with the application of a bias resulting in significant densification of the coating and a corresponding reduction in net deposition rate, effects that have been observed elsewhere in Cr-based coatings [26,29,30].

Regarding the XRD results, the Cr-coatings showed different peak intensities according to the bias applied. In general, the preferred peak was the (110) plane. As Gautier [33] discuss, the (110) plane is expected to be the preferred orientation due to its highest reticular density of

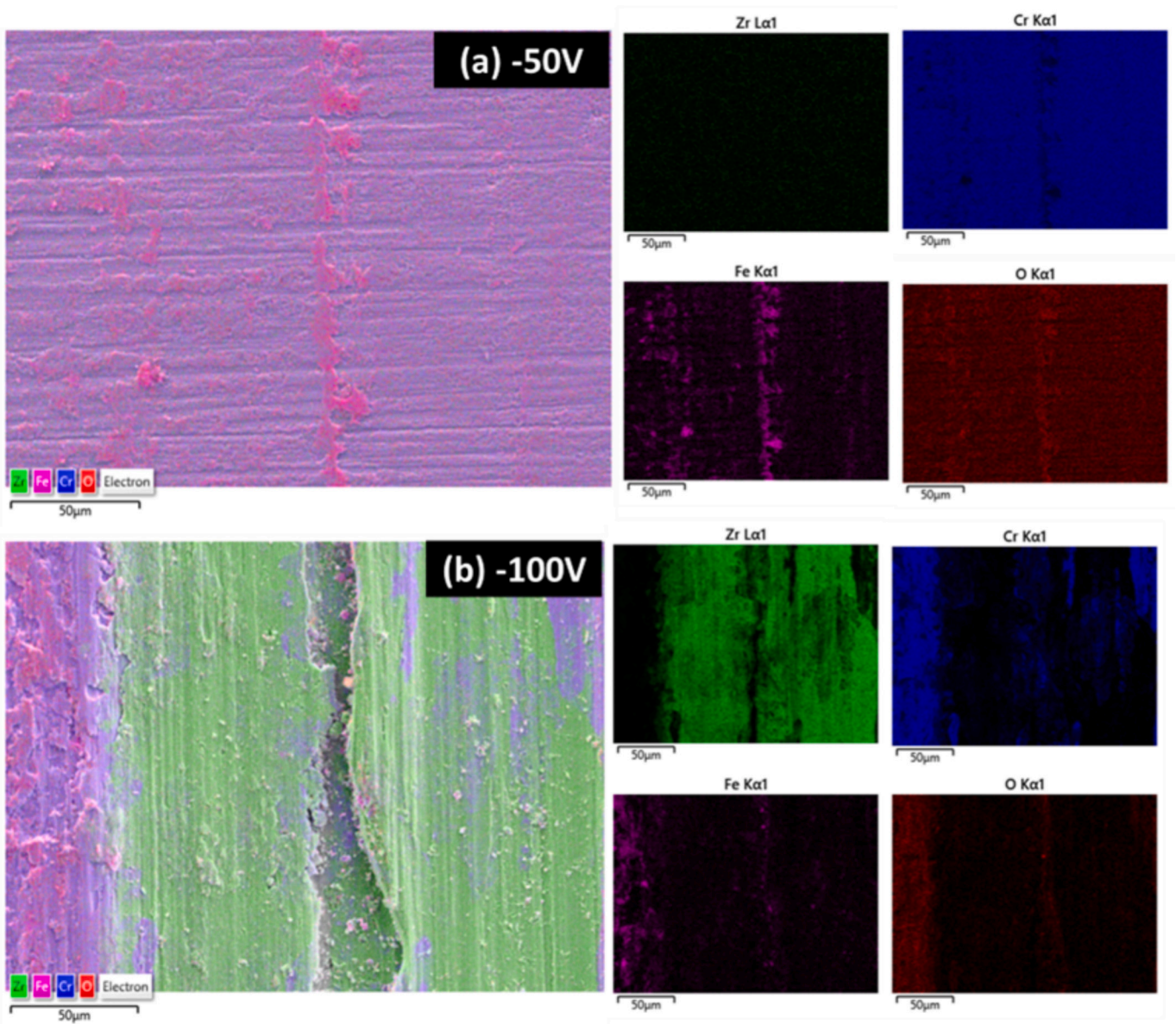


Fig. 10. EDX mapping analyses of the wear track at 5 N load test for Cr-coated samples under (a) –50 V, and (b) –100 V bias voltage.

1.414 atoms/ a^2 . In contrast, the other observed planes have lower densities, with the (200) plane at 1 atom/ a^2 and the (211) plane at 0.81 atoms/ a^2 . The findings in this work are consistent with these predictions [33].

The literature reports that highly textured thin films, like those seen in the NBA SEM images (Fig. 1(a)), often make detecting X-ray peaks in standard diffraction measurements challenging. Thin metal films tend to align their crystal structures to minimise interfacial energy, resulting in a pronounced texture in a specific direction—commonly the (111) planes in face-centred cubic (fcc) metals. Consequently, standard XRD scans primarily detect these aligned planes, while other crystal orientations may remain undetected [34].

To address this limitation, Borgia et al. proposed an alternative approach to the traditional XRD measurement in the plane orthogonal to the sample normal [34]. They introduced the use of the Eulerian cradle, a sample holder that allows multiple XRD scans along the $\theta/2\theta$ axis with precise control of the sample's orientation in 3D space. This technique allows precise orientation and alignment of the crystal sample. Their results demonstrated a significant improvement in peak intensities and the detection of additional peaks using this method. Based on these

findings, the single and low-intensity peak observed in the NBA sample appears to be a limitation of the equipment, as it may not adequately account for the strong texture present in the sample.

Additionally, some studies observed a shift in texture from the (110) to (200) plane as the bias rose [26,35,36], which was observed here, but only to a small degree. Meng [36] discussed the changes observed in the chromium texture using magnetron sputtering and varied bias. They mentioned that a gradual rise in the bias voltage negatively impacts chromium's crystallinity, reducing both (110) and (200) peaks. Wang [23] also reported a peak diminution with continuous bias increase for chromium coatings, mainly from –90 V to –150 V bias voltage [19]. Both studies cited above claimed that excessively high bias voltage leads to an overload of energy, which hampers the energy deposition process and obstructs the formation of the (110) texture.

Moreover, the texture evolution is highly dependent on the temperature, argon pressure and bias voltage. Feng [37] investigated deeply the effect of the crystallographic texture of Cr films varying some deposition parameters, including pressure, bias and heat of the substrate. They reported that higher temperatures benefited the (200) texture, while the bias promotes the (110) texture. Hence, the transition

to the (200) plane under high bias may also occur due to inherent surface heating resulting from increased bias levels. However, in this study, it appears that the bias effects were more relevant than the process heating caused by the bias, which was not significant regarding texture shift.

Therefore, the XRD suggest that, without applying a bias voltage, adatoms lack sufficient energy to diffuse and form a highly textured structure. As a result, only a limited number of peaks are observed. Introducing a bias voltage enhances the mobility of the adatoms and the kinetic energy when they reach the substrate, promoting a dense structure and the (110) texture. However, excessively high bias voltage leads to an overload of energy, which hampers the energy deposition process and obstructs the formation of the (110) texture.

In terms of hardness, the coating hardness increased from the non-biased condition (NBA) to -50 V but remained relatively constant at higher bias voltages of -100 V and -150 V. Various factors, including microstructure, grain size and internal stress, typically influence film hardness. Some of these factors were investigated in order to understand the observed hardness behaviour.

First, hardness of a material is negatively correlated with grain size according to the Hall-Petch relationship. Hardness increases because there are more grain boundaries in a structure with smaller grains. These boundaries behave as barriers to grain dislocation. Therefore, the movement of grains is restricted, and the plastic deformation is limited. As a result, the material's strength and hardness are enhanced.

In this work, the grain size measured through the STEM images shows a trend between grain size and hardness that follows the Hall-Petch relationship. The Cr coating deposited at -50 V exhibited the smallest grain size and higher hardness. In contrast, the grain size more than doubled for the samples deposited at -100 V and -150 V. The latter two samples demonstrated minimal differences in both hardness and grain size.

Meng [36] discuss a critical fact about the Cr (110) plane, how it is affected by bias voltage and its influence on the structure properties. Meng [36] study shows how bias voltage can influence the coating texture and be detrimental to the crystallinity at higher values. Also, they said it is worth modulating the chromium texture to achieve the highest reticular density. The most advantageous orientation for chromium coatings featuring body-centred cubic (BCC) lattices is the low-energy closed-packed (110) plane, which boasts the highest lattice density of 1.414 atoms/ \AA^2 . The (110) orientation is beneficial because the higher density of plane makes oxygen penetration difficult and protects the substrate better, which is advantageous for several applications [36].

In this study, the chromium coating subjected to a bias voltage of -50 V exhibited the most pronounced peak intensity at the (110) plane compared to other coatings. This observation was correlated with an increased level of hardness in the -50 V bias coating. Conversely, as the bias voltage was further raised to -100 V and -150 V, there was a noticeable reduction in the intensity of the (110) peak, accompanied by a decline in hardness. Consequently, it was observed that coatings possessing greater crystallinity in the (110) texture tended to exhibit higher levels of hardness. This phenomenon can likely be attributed to the enhanced lattice density of the (110) plane within the BCC structure, which may also contribute to the increased hardness at -50 V.

When comparing our findings with other studies examining the relationship between bias voltage and hardness in chromium (Cr) coatings, a consistent trend emerges. For instance, Chen [38] reported the highest hardness at a bias voltage of -150 V, corresponding to the presence of the (110) plane with the highest intensity [35]. Similarly, an investigation conducted by Wang [35] demonstrated higher hardness in a bias voltage of -90 V which exhibits greater crystallinity in the (110) texture [34]. It is essential to notice that the fabrication methods differed in these studies, with Chen [38] utilising High-Power Impulse Magnetron Sputtering (HIPIMS) and Wang [35] employing Radio Frequency Magnetron Sputtering (RFMG). These methodological

distinctions may contribute to variations in the observed characteristics concerning bias voltage and hardness.

4.2. Mechanical properties assessments: influence of substrate bias in coating wear resistance

The wear resistance of the chromium coatings was discussed in terms of their relative wear rates and wear depth provided in Fig. 5. First, it is noteworthy that the wear results correlate with the coatings' hardness (Table 2). The Cr-coating with the best performance – -50 V bias – presents the harder film. As expected, with its low hardness and porous structure, the NBA coating showed the worst protection. The coatings produced at -100 V and -150 V showed reasonable results at medium hardness. Furthermore, the coating deposited at -50 V bias voltage exhibited the highest H/E ratio, which supports its excellent performance in the wear tests. According to the literature, a higher H/E ratio is associated with greater wear resistance [32,39]. Similarly, Zhao [21] attributed the improved fretting corrosion resistance of Cr-coated Zr alloys to the increased hardness of the chromium. They also linked these results to the enhanced plasticity of metallic chromium.

It is noticed that the worn surfaces of the Cr-coated using different biases are different. First, the presence of iron on the chromium coatings indicates that initially, the wear is occurring on the ball rather than the coating itself. However, when the sample lacks sufficient hardness, the chromium wears away entirely, transferring zirconium (Zr) to the opposing surface. Adhesive wear, characterised by the transfer of material from one surface to another in localised areas, is observed in this system due to the material adherence between surfaces. Similarly, Dai [40] examined the fretting corrosion behaviour of Cr-coated Zr alloy claddings and also identified adhesive wear on the Cr coatings. Furthermore, they reported that once the Cr coating was entirely worn away, a ZrO_2 film formed on the underlying substrate.

Additionally, the presence of fine and long parallel grooves on the sliding surfaces of the coating suggests signs of abrasive wear, which occurs when a harder material removes material across a softer surface. However, the ball-bearing hardness specified by the fabricants is between 120 and 160 HB, representing about 2 GPa. Therefore, the ball material is softer than the coating and the substrate. This is inconsistent with the abrasive wear concept and also what is observed in the wear tracks here. Nevertheless, abrasive wear can also arise from hard particles from the Cr coating becoming trapped between the surfaces, a phenomenon known as 'three-body abrasive wear'. Third bodies consist of films and particles formed under high stress at the contact interface through tribo-mechanical processes. The effect of the third-body debris can increase friction by filling the wear track with debris.

As illustrated in the Fig. 9, the sample coated at -100 V bias voltage displayed parallel grooves running in the friction directions, in addition to the accumulation of debris. Interestingly, this coating exhibited more intensive wear. The severity of the wear correlates with the increased presence of groove lines and debris within the wear track. All indications suggest that abrasive wear occurs in the -100 V sample. Conversely, only debris was found on the worn surface in the sample treated with a -50 V bias voltage where minimal wear occurred, suggesting adhesive wear.

Wang [41] investigated the progression of fretting wear on Cr-coated cladding as the number of wear test cycles increased. During the initial stages, with fewer cycles, the worn area was minimal, and adhesive wear was the primary wear mechanism observed on the Cr surface. However, as the cycles increased, the worn area expanded, the coating was fully degraded, and the wear mechanism evolved into fatigue wear, abrasive wear, and delamination. Similarly, in this study, the bias conditions demonstrated a transition from adhesive to abrasive wear, progressing from mild damage at -50 V to severe damage at -100 V.

5. Conclusions

Chromium coatings of 6–7 μm were deposited by pulsed DC magnetron sputtering onto Zr alloy substrate under conditions of no bias applied, -50 V , -100 V , and -150 V substrate DC bias voltages. The application of a substrate bias during deposition resulted in significant film densification and modification to film crystallinity and mechanical properties. Findings are listed below:

- The Cr-coated ZIRLO™ notably enhanced sliding wear performance compared to uncoated ZIRLO™.
- All bias voltage coatings demonstrated some protection to the substrate in comparison with no coating.
- The Cr-coated ZIRLO™ at -50 V bias voltage presented the best performance in terms of wear resistance. The reasons to that may be higher hardness conferred by the smaller grain size and the higher crystallinity of the (110) texture, which have the highest atomic density among the Cr BCC planes.

CRedit authorship contribution statement

Thais R. Netto: Writing – original draft, Methodology, Investigation, Formal analysis, Data curation. **Adele K. Evans:** Writing – review & editing, Supervision, Investigation, Formal analysis. **David T. Goddard:** Supervision. **Jack L. Cooper:** Supervision. **Peter Kelly:** Writing – review & editing, Supervision, Investigation, Formal analysis.

Declaration of competing interest

The authors declare that they have no known competing financial interests or personal relationships that could have appeared to influence the work reported in this paper.

Acknowledgements

This work was supported by the Department for Energy Security and Net Zero's (DESNZ) £505 m Energy Innovation Programme for providing funding for the research under the £46 m Advanced Fuel Cycle Programme.

Data availability

Data will be made available on request.

References

- [1] J.M. Chen, Carbon neutrality: toward a sustainable future, *The Innovation* 2 (3) (2021) 100127, <https://doi.org/10.1016/j.xinn.2021.100127>.
- [2] M.D. Mathew, Nuclear energy: a pathway towards mitigation of global warming, *Progress in Nuclear Energy* 143 (2022), <https://doi.org/10.1016/j.pnucene.2021.104080>.
- [3] L. Liu, H. Guo, L. Dai, M. Liu, Y. Xiao, T. Cong, H. Gu, The role of nuclear energy in the carbon neutrality goal, *Prog. Nucl. Energy* 162 (2023), <https://doi.org/10.1016/j.pnucene.2023.104772>.
- [4] C. Tang, M. Stueber, H.J. Seifert, M. Steinbrueck, Protective coatings on zirconium-based alloys as accident-tolerant fuel (ATF) claddings, *Corrosion Rev.* 35 (2017) 3, <https://doi.org/10.1515/corrrev-2017-0010>.
- [5] K. Kim, Evolutionary developments of advanced PWR nuclear fuels and cladding materials, *Nuclear Engineering and Design* 263 (2013) 59–69, <https://doi.org/10.1016/j.nucengdes.2013.04.013>.
- [6] Z. Hu, Developments of analyses on grid-to-rod fretting problems in pressurized water reactors, *Progress in Nuclear Energy* 106 (2018) 293–299, <https://doi.org/10.1016/j.pnucene.2018.03.015>.
- [7] Z. Cai, Z. Li, M. Yin, M. Zhu, Z. Zhou, A review of fretting study on nuclear power equipment, *Tribol. Int.* 144 (2020) 106095, <https://doi.org/10.1016/j.triboint.2019.106095>.
- [8] T.C. Winter, R.W. Neu, P.M. Singh, L.E. Kolaya, C.S. Deo, Fretting wear comparison of cladding materials for reactor fuel cladding application, *Journal of Nuclear Materials* 508 (2018) 505–515, <https://doi.org/10.1016/j.jnucmat.2018.05.069>.
- [9] K. Kim, The study on grid-to-rod fretting wear models for PWR fuel, *Nuclear Engineering and Design* 239 (12) (2009) 2820–2824, <https://doi.org/10.1016/j.nucengdes.2009.08.018>.
- [10] S. Lazarevic, R.Y. Lu, C. Favade, G. Plint, P.J. Blau, J. Qu, Investigating grid-to-rod fretting wear of nuclear fuel claddings using a unique autoclave fretting rig, *Wear* 412–413 (2018) 30–37, <https://doi.org/10.1016/j.wear.2018.06.011>.
- [11] K.A. Terrani, Accident tolerant fuel cladding development: promise, status, and challenges, *J. Nucl. Mater.* 501 (2018) 13–30, <https://doi.org/10.1016/j.jnucmat.2017.12.043>.
- [12] D. Yun, C. Lu, Z. Zhou, Y. Wu, W. Liu, S. Guo, T. Shi, J.F. Stubbins, Current state and prospect on the development of advanced nuclear fuel system materials: a review, *Materials Reports: Energy* 1 (2021) 100007, <https://doi.org/10.1016/j.matre.2021.01.002>.
- [13] J. Yang, M. Steinbrück, C. Tang, M. Große, J. Liu, J. Zhang, D. Yun, S. Wang, Review on chromium coated zirconium alloy accident tolerant fuel cladding, *Journal of Alloys and Compounds* 895 (Part 1) (2022) 162450, <https://doi.org/10.1016/j.jallcom.2021.162450>.
- [14] Z. Duan, H. Yang, Y. Satoh, K. Murakami, S. Kano, Z. Zhao, J. Shen, H. Abe, Current status of materials development of nuclear fuel cladding tubes for light water reactors, *Nuclear Engineering and Design* 316 (2017) 131–150, <https://doi.org/10.1016/j.nucengdes.2017.02.031>.
- [15] T. Dabney, G. Johnson, H. Yeom, B. Maier, J. Walters, K. Sridharan, Experimental evaluation of cold spray FeCrAl alloys coated zirconium-alloy for potential accident tolerant fuel cladding, *Nuclear Materials and Energy* 21 (2019), <https://doi.org/10.1016/j.nme.2019.100715>.
- [16] R.V. Umretiya, B. Elward, D. Lee, M. Anderson, R.B. Rebak, J.V. Rojas, Mechanical and chemical properties of PVD and cold spray Cr-coatings on Zircaloy-4, *Journal of Nuclear Materials* 541 (2020), <https://doi.org/10.1016/j.jnucmat.2020.152420>.
- [17] E.B. Kashkarov, D.V. Sidelev, M. Rombaeva, M.S. Syrtanov, G.A. Bleykher, Chromium coatings deposited by cooled and hot target magnetron sputtering for accident tolerant nuclear fuel claddings, *Surf. Technol.* 389 (2020) 125618, <https://doi.org/10.1016/j.surfcoat.2020.125618>.
- [18] H. Yeom, B. Maier, G. Johnson, T. Dabney, J. Walters, K. Sridharan, Development of cold spray process for oxidation-resistant FeCrAl and Mo diffusion barrier coatings on optimized ZIRLO™, *Journal of Nuclear Materials* 507 (2018) 306–315, <https://doi.org/10.1016/j.jnucmat.2018.05.014>.
- [19] C. Wang, X. Li, A. Liang, Reverse V-shaped wear rate vs. friction velocity curve of hard chromium coating and its inspiration for anti-wear coating design, *Mater. Lett.* 330 (2023) 133369, <https://doi.org/10.1016/j.matlet.2022.133369>.
- [20] B. Reed, R. Wang, R.Y. Lu, J. Qu, Autoclave grid-to-rod fretting wear evaluation of a candidate cladding coating for accident-tolerant fuel, *Wear* 466–467 (2021) 203578, <https://doi.org/10.1016/j.wear.2020.203578>.
- [21] Y. Zhao, Y. Bai, J. Yang, Y. Shen, Y. Lou, K. Zhang, Y. Wu, Y. Li, J. Li, Z. Cui, T. Wei, S. Ma, Z. Shen, H. Wang, X. Zeng, Autoclave grid-to-rod fretting corrosion behaviors of the Zr alloy fuel cladding with and without Cr coating through advanced characterization, *Corrosion Science* 239 (2024) 112379, <https://doi.org/10.1016/j.corsci.2024.112379>.
- [22] P.J. Kelly, R.D. Arnell, Magnetron sputtering: a review of recent developments and applications, *Vacuum* 56 (3) (2000) 159–172, [https://doi.org/10.1016/S0042-207X\(99\)00189-X](https://doi.org/10.1016/S0042-207X(99)00189-X).
- [23] J.T. Gudmundsson, Physics and technology of magnetron sputtering discharges, *Plasma Sources Sci. Technol.* 29 (2020) 113001, <https://doi.org/10.1088/1361-6595/abb7bd>.
- [24] K.H. Müller, Model for ion-assisted thin-film densification, *J. Appl. Phys.* 59 (1986) 2803–2807, <https://doi.org/10.1063/1.336960>.
- [25] C.A. Davis, A simple model for the formation of compressive stress in thin films by ion bombardment, *Thin Solid Films* 226 (1993) 30–34, [https://doi.org/10.1016/0040-6090\(93\)90201-Y](https://doi.org/10.1016/0040-6090(93)90201-Y).
- [26] P.A. Mouche, A. Evans, W. Zhong, T. Koyanagi, Y. Katoh, Effects of sample bias on adhesion of magnetron sputtered Cr coatings on SiC, *J. Nucl. Mater.* 556 (2021) 153251, <https://doi.org/10.1016/j.jnucmat.2021.153251>.
- [27] X. He, Z. Tian, B. Shi, X. Xu, C. Meng, W. Dang, J. Tan, X. Ma, Effect of gas pressure and bias potential on oxidation resistance of Cr coatings, *Ann. Nucl. Energy* 132 (2019) 243–248, <https://doi.org/10.1016/j.anucene.2019.04.038>.
- [28] S.K. Ray, A. Banerjee, B.K. Bhangui, D. Pyne, B. Dutta, Tribological analysis—general test standards, in: *Tribology of Polymers, Polymer Composites, and Polymer Nanocomposites*, 2022, pp. 17–50, <https://doi.org/10.1016/B978-0-323-90748-4.00001-7>.
- [29] K. Aouadi, et al., Influence of substrate bias voltage on corrosion and wear behavior of physical vapor deposition CrN coatings, *Journal of Materials Engineering and Performance* 28 (2019) 2881–2891, <https://doi.org/10.1007/s11665-019-04033-y>.
- [30] Z. Wang, D. Zhang, P. Ke, X. Liu, A. Wang, Influence of substrate negative bias on structure and properties of TiN coatings prepared by hybrid HIPIMS method, *Journal of Materials Science & Technology* 31 (2015) 37–42, <https://doi.org/10.1016/j.jmst.2014.06.002>.
- [31] P. Zhu, et al., Effect of bias voltage on the microstructure, mechanical properties, and high-temperature steam oxidation behavior of Cr coatings prepared by magnetron sputtering on Zircaloy-4 alloy, *J. Mater. Eng. Perform.* 33 (17) (2023) 8627–8640, <https://doi.org/10.1007/s11665-023-08554-5>.
- [32] A. Leyland, A. Matthews, On the significance of the H/E ratio in wear control: a nanocomposite coating approach to optimised tribological behaviour, *Wear* 246 (2000) 1–11, [https://doi.org/10.1016/S0043-1648\(00\)00488-9](https://doi.org/10.1016/S0043-1648(00)00488-9).
- [33] G. Gautier, J. Machet, Effects of deposition parameters on the texture of chromium films deposited by vacuum arc evaporation, *Thin Solid Films* 289 (1996) 34–38, [https://doi.org/10.1016/S0040-6090\(96\)08891-8](https://doi.org/10.1016/S0040-6090(96)08891-8).
- [34] C. Borgia, S. Olliges, R. Spolenak, Rapid qualitative phase analysis in highly textured thin films by x-ray diffraction, *Rev. Sci. Instrum.* 79 (2008) 043904, <https://doi.org/10.1063/1.2907534>.

- [35] W. Wang, G. Zhang, C. Wang, T. Wang, Y. Zhang, T. Xin, Construction of Cr coatings with different columnar structure on Zircaloy-4 alloys to optimize the high-temperature steam oxidation behavior for accident tolerant fuel claddings, *J. Alloys Compd.* 946 (2023), <https://doi.org/10.1016/j.jallcom.2023.169385>.
- [36] Y. Meng, S. Zeng, Z. Teng, X. Han, H. Zhang, Control of the preferential orientation Cr coatings deposited on zircaloy substrates and study of their oxidation behavior, *Thin Solid Films* 730 (2021) 138699, <https://doi.org/10.1016/j.tsf.2021.138699>.
- [37] Y.C. Feng, D.E. Laughlin, Formation of crystallographic texture in rf sputter-deposited Cr thin films, *J. Appl. Phys.* 76 (1994).
- [38] Q.S. Chen, C.H. Liu, R.Q. Zhang, H.Y. Yang, T.G. Wei, Y. Wang, Z. Li, L.X. He, J. Wang, L. Wang, J.P. Long, H. Chang, Microstructure and high-temperature steam oxidation properties of thick Cr coatings prepared by magnetron sputtering for accident tolerant fuel claddings: the role of bias in the deposition process, *Corros. Sci.* 165 (2020) 108378, <https://doi.org/10.1016/j.corsci.2019.108378>.
- [39] A. Kumar, D.Y. Li, Can the H/E ratio be generalized as an index for the wear resistance of materials? *Mater. Chem. Phys.* 275 (2022) 125245 <https://doi.org/10.1016/j.matchemphys.2021.125245>.
- [40] G. Dai, J. Yan, X. Liang, Y. Li, Z. Peng, J. Xue, L. Xin, X. Lin, Y. Liao, Q. Li, Fretting corrosion behavior of a Cr-coated Zr-1Nb alloy cladding in simulated PWR primary water environment, *Corros. Sci.* 233 (2024) 112065, <https://doi.org/10.1016/j.corsci.2024.112065>.
- [41] J. Wang, K. Li, Y. Wu, Y. Xie, J. Ni, Z. Zhu, Z. Cai, Evolution of fretting wear characteristics of Cr-coated cladding under high-temperature pressurized water environment, *Nucl. Eng. Des.* 430 (2024) 113665, <https://doi.org/10.1016/j.nucengdes.2024.113665>.